

Pasadena: Perceptually Aware and Stealthy Adversarial Denoise Attack

Yupeng Cheng*
Nanyang Technological University
Singapore

Qing Guo*[†]
Nanyang Technological University
Singapore

Felix Juefei-Xu
Alibaba Group
USA

Xiaofei Xie
Nanyang Technological University
Singapore

Shang-Wei Lin
Nanyang Technological University
Singapore

Weisi Lin
Nanyang Technological University
Singapore

Wei Feng
Tianjin University
China

Yang Liu
Nanyang Technological University
Singapore

ABSTRACT

Image denoising techniques have been widely employed in multimedia devices as an image post-processing operation that can remove sensor noise and produce visually clean images for further AI tasks, *e.g.*, image classification. In this paper, we investigate a new task, *adversarial denoise attack*, that stealthily embeds attacks inside the image denoising module. Thus it can simultaneously denoise input images while fooling the state-of-the-art deep models. We formulate this new task as a kernel prediction problem and propose the *adversarial-denoising kernel prediction* that can produce adversarial-noiseless kernels for effective denoising and adversarial attacking simultaneously. Furthermore, we implement an adaptive *perceptual region localization* to identify semantic-related vulnerability regions with which the attack can be more effective while not doing too much harm to the denoising. Thus, our proposed method is termed as *Pasadena* (Perceptually Aware and Stealthy Adversarial DENoise Attack). We validate our method on the NeurIPS'17 adversarial competition dataset and demonstrate that our method not only realizes denoising but has advantages of high success rate and transferability over the state-of-the-art attacks.

KEYWORDS

adversarial denoise attack, image denoising, adversarial attack

1 INTRODUCTION

Although the imaging quality of various multimedia devices, *e.g.*, mobile phones and digital cameras, has been significantly improved by using more advanced sensors, image noise is still inevitable due to complex application situations, *e.g.*, low light conditions. As a result, image denoising techniques are widely employed as an image post-processing operation that can not only remove sensor noise and produce visually clean images but also can benefit the state-of-the-art AI-related tasks, *e.g.*, image classification [22].

The main sources of noise in multimedia digital images arise during the image acquisition and/or transmission stages. For example, when acquiring images with a CCD/CMOS camera, the sensor

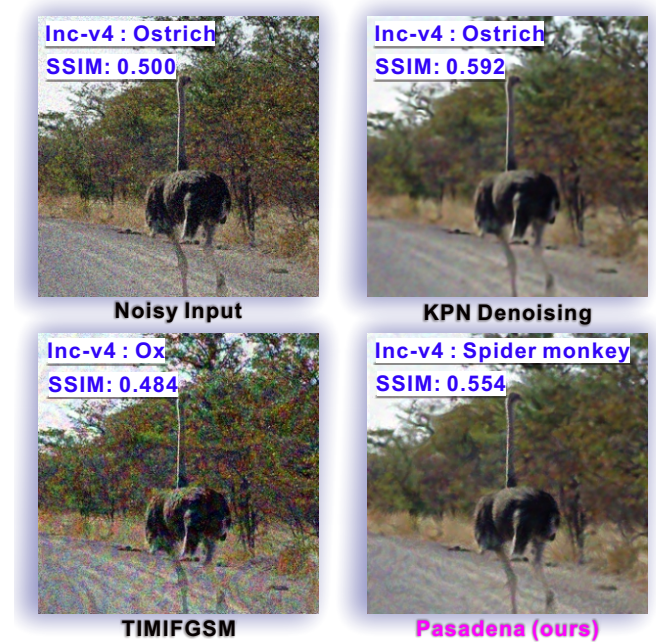


Figure 1: CNNs, *e.g.*, Inc-v4, are robust to natural noise, *e.g.*, Gaussian noise, and predict an object's category even with noisy input. State-of-the-art denoising methods, *e.g.*, kernel prediction network (KPN) [25], can improve the quality of noisy input and are usually helpful to AI tasks, *e.g.*, image classification. Existing adversarial attacks, *e.g.*, TIMIFGSM [7], can mislead CNNs while corrupting the image. Our method *Pasadena* can mislead the CNNs while improving the image quality, which makes attacks more practical for noisy inputs that are usually caused by low-quality sensors.

temperature are one of the major factors affecting image noise. Also, during wired or wireless digital image transmission process, the images can be further noise corrupted due to channel interference or other atmospheric disturbance.

To restore the corrupted image by performing image denoising, traditional methods rely heavily on fixed hand-crafted spatial filters, such as mean filters (arithmetic mean, geometric mean, harmonic mean, *etc.*), median filter, min and max filters, *etc.* More recently, learning based filters for image denoising have become more and more popular such as [2] and [25].

*Both authors contributed equally to this research.

[†]Qing Guo is the corresponding author (qing.guo@ntu.edu.sg).

In this work, we are investigating a novel vulnerability during the image post-processing pipeline by stealthily embedding the attacks inside the denoising module. The resulting image is not only a denoised version of itself, but also can fool the state-of-the-art deep image classification models at the same time. We formulate this new task as a kernel prediction problem and propose the *adversarial-denoising kernel prediction* that can produce adversarial-noiseless kernels for effective denoising and adversarial attacking simultaneously. Furthermore, we implement an adaptive *perceptual region localization* to identify the semantic-related vulnerability regions with which the attack can be more effective while not doing too much harm to the denoising. Thus, our proposed method is termed as *Pasadena* (Perceptually Aware and Stealthy Adversarial DENoise Attack). As illustrated in Fig. 1, (top left) what is shown here is that CNNs, e.g., Inc-v4, are robust to natural noise, e.g., Gaussian noise, and usually can predict an object's category correctly even with noisy input. (Top right) the state-of-the-art denoising methods such as the kernel prediction network (KPN) [25] can improve the quality of noisy input and are usually helpful to AI tasks, e.g., image classification. (Bottom left) existing adversarial attacks, e.g., TIM-IFGSM [7], can mislead CNNs while corrupting the image. (Bottom right) our proposed method, *Pasadena*, can not only mislead CNNs but also at the same time improve the image quality, which makes attacks more practical for noisy inputs that are usually caused by low-quality sensors.

We have validated our method on the NeurIPS'17 adversarial competition dataset and demonstrate that our method not only realizes denoising but has advantages of high success rate and transferability over the state-of-the-art attacks. More specifically, our method improve the image quality for over 0.1 in SSIM evaluation criterion with a comparable attack success rate. When the image qualities of our results decrease to similar level with the other attack methods, they still maintain the whitebox attack success rate and show better blackbox attack transferability. To the best of our knowledge, this is the very first successful attempt to carry out simultaneous image denoising and denoise attack. Our main contributions are summarized as follows:

- We have identified and investigated a novel type of adversarial attack: the adversarial denoise attack.
- We have devised a novel method to embed the attacks inside the image denoising module. Therefore, it can simultaneously denoise the input images while making the denoised images fool the state-of-the-art deep image classification models.
- We have formulated this new task as a kernel prediction problem and proposed the *adversarial-denoising kernel prediction* that can produce adversarial-noiseless kernels for effective denoising and adversarial attacking simultaneously.
- We have implemented an adaptive *perceptual region localization* to identify the semantic-related vulnerability regions with which the attack can be more effective while not doing too much harm to the denoising.
- We have validated our method on the NeurIPS'17 adversarial competition dataset and demonstrate that our method not only realizes denoising but has advantages of high success rate and transferability over the state-of-the-art attacks.

2 RELATED WORK

2.1 Image Denoising

Image noise is inevitable during the signal acquisition and transmission, which makes image denoising become fundamental for many signal processing or computer vision tasks, such as visual enhancement, feature extraction, and face recognition [23, 33]. Many classic methods address it as a statistic problem using analytical priors [31, 35]. BM3D [5], as one of the most widely used algorithms, try to estimate the true signal by collaborative filtering several similar image fragments and enhancing their sparsity in frequency domain. Similarly, Guo *et al.* [12] use the low-rank approximation (LRA) to estimate and depress the noise in patches. Based on the same assumption that similar noisy patches can be averaged to better estimate the true signal, multi-image denoising techniques including video or burst images were built, such as VBM4D [24]. It align similar image patches and jointly filter them by robust averaging. Nevertheless, other researchers focus on the high image quality. They utilize the capability of CNN techniques, addressing these tasks as optimization problem [15, 16]. But, these works still need alignment prediction in forward model.

Kernel-prediction networks [2] denoise Monte Carlo renderings with a learned pre-pixel kernel map. They shift alignment calculation from input images to kernel. Inspired by this work, Mildenhall *et al.* [25] denoises image burst by generating kernel maps for all burst images. In that way, blurry artifacts in common direct pixel predict networks are constrained.

2.2 Adversarial Attacks

The success of deep learning facilitates many computer vision classic tasks. Except for denoising [4, 47], deblurring [37], demosaicking [8], and super-resolution [41] also propose many deep based solution. With the improvements of neural network [14, 18, 39], it starts to enter safety and security critical applications [1, 17, 29, 30, 34]. However, Szegedy *et al.* [40] discovers that a carefully crafted input, named adversarial example, can mislead a well trained deep model generating wrong prediction with high confidence.

Let \mathbf{X} denotes a clean image, and let $\phi(\cdot)$ denotes the DNNs classifier which is known by the adversary. The goal of adversarial attacking is to generate adversarial noise \mathbf{E} under some constraint limiting its ℓ_p norm $\|\mathbf{E}\|_p$, such that prediction w.r.t. the resultant image $\hat{\mathbf{X}} = \mathbf{X} + \mathbf{E}$ becomes incorrect. The choice of p is different in attacking methods [9, 27, 36]. Specifically, Goodfellow *et al.* [9] proposed a low computational cost attack method fast gradient sign method (FGSM) based on ℓ_∞ norm. Moreover, as a typical ℓ_2 norm adversarial method, DeepFool [27] computes adversarial examples with tiny distortion through a simple and accurate way regardless of time consumption. Besides, Su *et al.* [36] presented an extreme ℓ_0 norm method indicating that merely one pixel's modification can totally confuse the neural networks classifier. Apart from these while-box attacks, where the model is directly accessible by the adversary, another line of work focus on enhancing the transferability of adversary. This ability enable adversarial examples crafted for one model to fool another model. In that case, the so called black-box attacks can disturb real-world model and draws many severe consequences. FGSM is a powerful whitebox adversary, and so is

its iteration version I-FGSM. But they both have poor performance under the setting of black-box. Dong *et al.* [6] upgrade this attack by integrating momentum in each iteration. It can stabilize the update direction and thereby enhance the transferability of adversarial examples. Moreover, Xie *et al.* [46] improves the transferability by realizing an increase in respect of input diversity. Inspired by data augmentation techniques, they resize and translate the images under a fixed probability to overcome the over-fitting of adversary.

Real-world photos have intrinsic noise, and denoising is a common image processing step. As mentioned above, majority of adversarial examples are additive noise patterns. Some researchers hence utilize the denoising techniques to defense adversarial examples [28]. However, in this paper, we are proposing a new task combining denoising and adversarial attack to explore if attackers can take advantage of the denoising module.

3 METHOD

3.1 Problem Formulation

Given a noisy image X^n , we aim to produce an adversarial-noiseless image, *i.e.*, X^a , that can fool a deep model while having higher quality than X^n . We name this task as *adversarial denoise attack*.

We first review recent works on kernel-prediction-based image processing [2, 25]

$$X_p^a = g(X_p^n, k_p) = \sum_{q \in \mathcal{N}(p)} X_q^n k_{pq}, \quad (1)$$

where p denotes the p th noisy pixel in X^n , $\mathcal{N}(p)$ is the set of p 's neighbor pixels and has size of N , *i.e.*, p has N neighbor pixels including itself. Then, we can process the noisy pixel by linear combining its neighbor pixels where the combination weights are determined by a kernel, *i.e.*, $k_p = \{k_{pq} | q \in \mathcal{N}(p)\}$. Different pixels in X^n can have different kernels and we denote the all kernels as $\mathcal{K} = \{k_p\}$. Intuitively, the kernels determine the way to handle a noisy image. For example, when we let the values of k_p follow a Gaussian distribution that has highest value at k_{pp} , Eq. 1 becomes a Gaussian denoising method. More recent works [2, 25] offline train a convolutional neural network (CNN) to predict a kernel for each noisy pixel and realize much better denoising results.

To realize *adversarial denoise attack*, we decompose $\mathcal{K} = \{k_p\}$ into two parts, *i.e.*, adversarial kernel $\mathcal{K}^a = \{k_p^a\}$ and denoise kernel $\mathcal{K}^n = \{k_p^n\}$. The first kernel aims to generate an adversarial example that can fool deep models while the second one is to improve the noisy image's quality. We then reformulate Eq. 1 as

$$X_p^a = g(X_p^n, M_p, k_p^a, k_p^n) = \sum_{q \in \mathcal{N}(p)} X_q^n (M_p k_{pq}^a + (1 - M_p) k_{pq}^n), \quad (2)$$

where M is a perceptually-aware weight map with its values ranging from 0 to 1 and M_p denotes the p th pixel of M . Intuitively, M_p indicates if the p th pixel should be denoised or attacked. For example, if $M_p = 1$, $X_p^a = \sum_{q \in \mathcal{N}(p)} X_q^n k_{pq}^a$, which means X_p^a is set to fool deep models, otherwise, it is a denoised pixel.

When using Eq. 2 to produce noiseless while adversarial examples, we should consider the following problems: 1) Given a noisy image, how to estimate the adversarial kernel, *i.e.*, \mathcal{K}^a , and denoise kernel, *i.e.*, \mathcal{K}^n , effectively? 2) How to estimate the perceptually

aware weight map, *i.e.*, M , which should be sparse (*i.e.*, to make sure most of image regions be denoised) and perceptual (*i.e.*, to make sure semantic-dependent regions be attacked). We will detail solutions of the two issues in Section 3.2 and 3.3 and summarize the attack algorithm in Section 3.4.

3.2 Adversarial-Denoising Kernel Prediction

Given a deep model for image classification denoted as $\phi(\cdot)$ and a noisy image X^n , we can predict the classification label y of the image via $\phi(X^n)$. Our attack method is to generate an adversarial-noiseless example, *i.e.*, X^a , which can let the deep model predict an incorrect label.

First, to denoise the noisy image, we propose to estimate the denoise kernel, *i.e.*, $\mathcal{K}^n = \{k_p^n\}$, through recent kernel-prediction-based denoising method [25]. It takes noisy images as input and trains a pretrained CNN to predict spatially varying denoise kernels that can remove a wide range of noise.

Second, to realize effective attack, we build the following objective function and optimize it to get the required adversarial kernels, *i.e.*, $\mathcal{K}^a = \{k_p^a\}$, as well as the weight map $M = \{M_p\}$:

$$\begin{aligned} \arg \max_{M, \mathcal{K}^a} & \lambda J_1(\phi(\{g(X_p^n, M_p, k_p^a, k_p^n)\}), y) - (1 - \lambda) J_2(\mathcal{K}^a, \mathcal{K}^n) \\ & \text{subject to } \forall p, \|k_p^a\|_0 \leq \epsilon, \end{aligned} \quad (3)$$

where $J_1(\cdot)$ denotes the crossing entropy loss for the objective of generating adversarial kernels, *i.e.*, fooling the deep model $\phi(\cdot)$, and $J_2(\cdot)$ is the L_2 norm loss that encourages the adversarial kernels $\{k_p^a\}$ similar to the denoise kernels $\{k_p^n\}$ to produce a high quality image. The hyper-parameter λ controls the balance between two loss functions. The ' \cdot ' means the set of pixel-depended variables. For example, $\{g(X_p^n, M_p, k_p^a, k_p^n)\}$ is the set of X^a 's pixels. Each pixel of X^n has an adversarial kernel, *e.g.*, k_p^a , and a weight, *e.g.*, M_p .

The constrain term, *i.e.*, $\|k_p^a\|_0 \leq \epsilon$, requires the size of k_p^a should not be larger than ϵ . An oversize kernel lets the attack success easily but heavily corrupts the original noisy image with worse quality.

We can calculate the gradient of the objective functions with respect to both adversarial kernels and the weight map, thus realize the gradient-based whitebox attack. We will show that such attack can also get high success rate under blackbox attacks. However, it should be note the weight map is only tuned by the objective of maximising the loss function, which helps achieve high success rate but harms the effectiveness of denoising. A desired strategy is to only attack semantic-related regions while denoising other regions to guarantee the image quality could be improved.

3.3 Perceptual Region Localization

As introduced in Sec. 3.1, the weight map M should be sparse and perceptual to realize effective *adversarial-denoise attack*. However, tuning the weight map $M = \{M_p\}$ by solving Eq. 3 directly cannot achieve these goals. In this section, we propose a perceptual region locator to produce sparse and perceptual M .

We first use a state-of-the-art perceptual edge detector, *i.e.*, bi-directional cascade network [13], to extract multi-scale edge maps of the input noisy image, *i.e.*, $\{E^i\}_{i=1}^N = \phi(X^n)$ where $\phi(\cdot)$ is the bi-directional cascade network and $\{E^i\}_{i=1}^N$ denote edge detection results of N scales. Then, we get $M = \{M_p\}$ by combining these

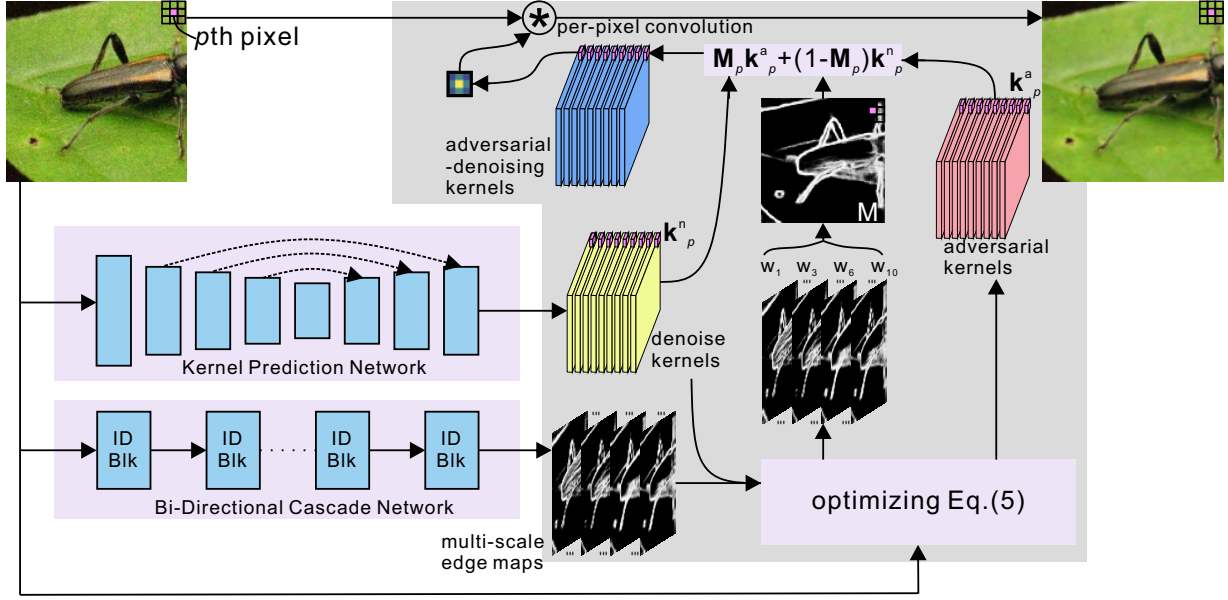


Figure 2: Pipeline of our Pasadena for adversarial denoise attack. *First*, we propose the *adversarial-denoising kernel prediction* where the adversarial kernels are predicted by optimizing the proposed adversarial objective function and the denoise kernels are calculated by employing a pre-trained kernel prediction network (KPN) [25]. *Second*, we propose the *perceptual region localization* where the semantic-related vulnerability regions are extracted by fusing multi-scale edge maps estimated by pre-trained bi-directional cascade network (BDCN) [13].

edge maps via

$$\mathbf{M}_p = \text{Sigmoid} \left(\sum_{i=1}^N w_i \mathbf{E}_p^i - \theta \right) \quad (4)$$

where \mathbf{E}_p^i and \mathbf{M}_p are the p th pixel of \mathbf{E}^i and \mathbf{M} , respectively. $\text{Sigmoid}(\cdot)$ is a general activation function mapping the output to $[0, 1]$. θ is a threshold. The intuitive motivation behind the idea is that the multi-scale edges are sparse (*i.e.*, most of the pixels of each edge map are labeled as zero, *i.e.*, non-edge) and perceptual (*i.e.*, covering the main semantic information). As a result, their linear combination, *i.e.*, our desired weight map, is naturally inherit these properties. Then, we can reformulate objective function in Eq. 3 as

$$\begin{aligned} \arg \max_{\{w_i\}, \mathcal{K}^a} & \lambda J_1(\phi(\{g(\mathbf{X}_p^n, \sum_{i=1}^N w_i \mathbf{E}_p^i, \mathbf{k}_p^a, \mathbf{k}_p^n)\}), y) - (1 - \lambda) J_2(\mathcal{K}^a, \mathcal{K}^n) \\ & \text{subject to } \forall p, \|\mathbf{k}_p^a\|_0 \leq \epsilon. \end{aligned} \quad (5)$$

3.4 Attack Algorithm

We summarize the whole process of our attack method in Algorithm 1. Given a noisy image \mathbf{X}^n , we first estimate the denoise kernels via kernel-prediction network (KPN), and the multi-scale edge maps via the bi-directional cascade network (BDCN). Then, we obtain the adversarial-noiseless image, *i.e.*, \mathbf{X}^a , by optimizing Eq. 5 with the hyper-parameters, *i.e.*, the kernel size $\epsilon = 5$, loss weight $\lambda = 0.9$, step size $\alpha = 0.1$, and iteration number $T = 10$. Among these parameters, the loss weight plays a key role for the balance between attack success rate and image quality and we will discuss the influence of the loss weight in the experimental section.

Algorithm 1: Pasadena for Adversarial Denoise Attack

Input: A noisy image \mathbf{X}^n ; the pre-trained kernel-prediction network (KPN); the pre-trained bi-directional cascade network (BDCN), *i.e.*, $\phi(\cdot)$; the attacked model $\phi(\cdot)$; hyper-parameters: $\epsilon = 5$, $\lambda = 0.9$, the threshold $\theta = 0.45$, step size $\alpha = 0.1$, and iteration number $T = 10$.

Output: Adversarial-noiseless image, *i.e.*, \mathbf{X}^a .

Predict the denoise kernels $\mathcal{K}^n = \text{kpn}(\mathbf{X}^n)$;
 Estimate the multi-scale edge maps $\{\mathbf{E}^i\}_{i=1}^N = \phi(\mathbf{X}^n)$;
 Randomly initialize the $\{w_i\}$ in the range $[0, 1]$ and $\sum_i w_i = 1$;
 Initialize the $\mathcal{K}^a = \mathcal{K}^n$;
 Obtain the ground truth label by $y = \phi(\mathbf{X}^n)$;

for $t = 1$ to T **do**

 Calculate the gradient of the objective functions in Eq. 5
 w.r.t. $\{w_i^t\}$ and $\mathcal{K}^{a,t}$ and get $\{\nabla w_i^t\}$ $\{\nabla \mathbf{k}_p^{a,t}\}$;

 Update $\{w_i\}$ and \mathcal{K}^a by $\{w_i^{t+1} = w_i^t + \alpha \nabla w_i^t\}$ and
 $\{\mathbf{k}_p^{a,t+1} = \mathbf{k}_p^{a,t} + \alpha \nabla \mathbf{k}_p^{a,t}\}$;

 Calculate the perceptual weight map by
 $\{\mathbf{M}_p^{t+1} = \text{Sigmoid}(\sum_{i=1}^N w_i^{t+1} \mathbf{E}_p^i - \theta)\}$;

 Calculate the adversarial-noiseless image by

$\{\mathbf{X}_p^a = g(\mathbf{X}_p^n, \mathbf{M}_p^{t+1}, \mathbf{k}_p^{a,t+1}, \mathbf{k}_p^n)\}$;

if $\phi(\mathbf{X}^a) \neq y$ **then**

 return \mathbf{X}^a ;

$t = t + 1$;

4 EXPERIMENTS

In this section, we illustrate our experimental results to demonstrate the capability of our framework in adversarial attacking while increasing the image quality. We first describe the experimental settings in Sec. 4.1. Afterwards, we compare the results of our framework with six baseline methods applying on noisy images in Sec. 4.2. Then, we also compare our method with a naive solution for joint denoising and attack, which generates another six baselines, in Sec. 4.3. At last, we perform the ablation study to evaluate the contribution of each component in Sec. 4.4.

4.1 Setup

Dataset and Models: We conduct our experiments on an ImageNet-compatible adversarial testing dataset [21]. This dataset was used in NIPS2017 adversarial competition and many recent adversarial works [7]. Specific to our task, we manually add Gaussian white noise ($\sigma = 0.1$) to the clean images to test the image quality increasing as well as the attack success of the adversarial attack methods. To verify our performance in various networks, we introduce three normally trained models, including Inception v3 (Inc-v3) [39], Inception v4 (Inc-v4) and Inception ResNet v2 (IncRes-v2) [38].

Metrics. To evaluate the effectiveness of the *adversarial denoise attack*, which fools classifier and denoises image at the same time, we select the attack success rate and image quality for measuring the performance of attack methods. There are two widely used full-reference image quality assessment metrics: peak signal-to-noise ratio (PSNR) and structural similarity (SSIM) [45]:

$$\text{PSNR}(X, Y) = 20 \cdot \log_{10} \left(\frac{\text{MAX}_I}{\text{MSE}} \right) \quad (6)$$

$$\text{SSIM}(X, Y) = \frac{(2\mu_x\mu_y + c_1)(2\sigma_{xy} + c_2)}{(\mu_x^2 + \mu_y^2 + c_1)(\sigma_x^2 + \sigma_y^2 + c_2)}, \quad (7)$$

where X and Y are two images. μ_x and μ_y are mean values of X and Y . σ_x^2 and σ_y^2 are variances of them. σ_{xy} is their covariance. MAX_I is the max value of intensity, which is 255 under 8-bit representation.

Due to that PSNR evaluates image via error sensitivity, it ignores the local structure information and results in a anti-subjective feeling. Thus, we propose a variant of PSNR which is denoted as PSNR_L . It measures the global signal difference and the local similarity at meantime with the help of a sliding window W . Given two images X, Y , their PSNR_L is formulated as:

$$\text{PSNR}_L(X, Y) = \frac{1}{S} \sum_{i=1}^S \text{PSNR}(W_i^X, W_i^Y), \quad (8)$$

where, W_i^X and W_i^Y are image patches of X and Y on the i th sliding window. S is the number of sliding windows. During the implementation, the sliding windows have a size of 8 and stride of 1. Besides, we also choose a no-reference image quality assessment metric, dubbed blind/referenceless image spatial quality evaluator (BRISQUE) [26], to further evaluate the quality of attack output. This metric utilizes scene statistics of locally normalized luminances coefficients, named mean subtracted contrast normalized (MSCN), to quantify possible losses of ‘naturalness’ in the image. Given an

image X , the MSCN coefficient on pixel $X(i, j)$ is formulated as:

$$\text{MSCN}(i, j) = \frac{X(i, j) - \mu(i, j)}{\sigma(i, j) + C}, \quad (9)$$

where, $i \in 1, 2, \dots, M, j \in 1, 2, \dots, N$ are indices, M, N are image height and width. $C = 1$ is a stability keeping constant parameter when the denominator tends to zero. $\mu(i, j)$ and $\sigma(i, j)$ are local weighted mean and local weighted standard deviation, respectively. Noted that, different with PSNR_L or SSIM, the lower BRISQUE value refers to better image quality. Finally, we select the attack success rate, PSNR_L , SSIM and BRISQUE for measuring the general performance of attack methods in our task.

Attack Baselines. We select six adversarial attack methods as the baselines: fast gradient sign method (FGSM) [9], momentum iterative fast gradient sign method (MIFGSM) [6], diverse inputs method (DIM) [46], as well as their translation-invariant version proposed in [7] which are denoted as TIFGSM, TIMIFGSM, and TIDIM, respectively. In particular, we set the Gaussian kernel (kernel size = 15 and $\sigma = 3$) following Dong’s report [7].

Denoise & Attack Baselines. We also compare our method with a naive solution for joint denoising and attack, *i.e.*, first denoising the noisy inputs and then attacking the denoised images. As a result, we obtain another six baselines (*i.e.*, ‘Denoise+FGSM/MIFGSM/DIM/TIFGSM/TIMIFGSM/TIDIM’) with the six attacks and a state-of-the-art denoising method, *i.e.*, KPN [25].

4.2 Comparison with Attack Baselines

4.2.1 Quantitative Analysis. We first demonstrate the denoising and attack ability of our framework in this part by evaluating the performance of adversarial examples crafted for Inc-v4 model. To evaluate the effect of our hyper-parameters, we choose four different adversarial weights λ in Eq. 3 ($\lambda = 0.9, 0.5, 0.3, 0.1$). The curves are generated by sliding threshold θ in Eq. 4 from 0.05 to 0.65. We also attack Inception-v4 model with six baseline adversarial methods. The maximum perturbation ϵ ranges from 4 to 55 with the max intensity of 255.

Fig. 4 illustrates the whitebox attacks against to Inc-v4 model. It seems that the baselines can keep their image quality with a small perturbation (See the rightmost two points of baselines.). However, this phenomenon is not an evidence of their image quality keeping ability. Because of the original noise of inputs, their image quality doesn’t decrease before adversarial noise level exceed the original noise level. But, when baseline methods attack images with ϵ over 8, the increase of ϵ then results in a rapid decrease on SSIM and PSNR_L (increase on BRISQUE), showing their negative effect against to image quality. On the other hand, our attack results have better image qualities comparing with all baselines. Even the point with highest success rate, which means a maximum perturbation strength, still have a higher SSIM or PSNR_L value (lower BRISQUE value). It demonstrates that our framework can achieve a similar attack ability with baselines, while having the potential to increase the image quality as well.

The curves of our methods with different weight settings show that lower threshold for edge detector refers to lager attack size in image, and thereby generates stronger attack. In addition, the adversarial loss weight determines the upper bound of attack ability.

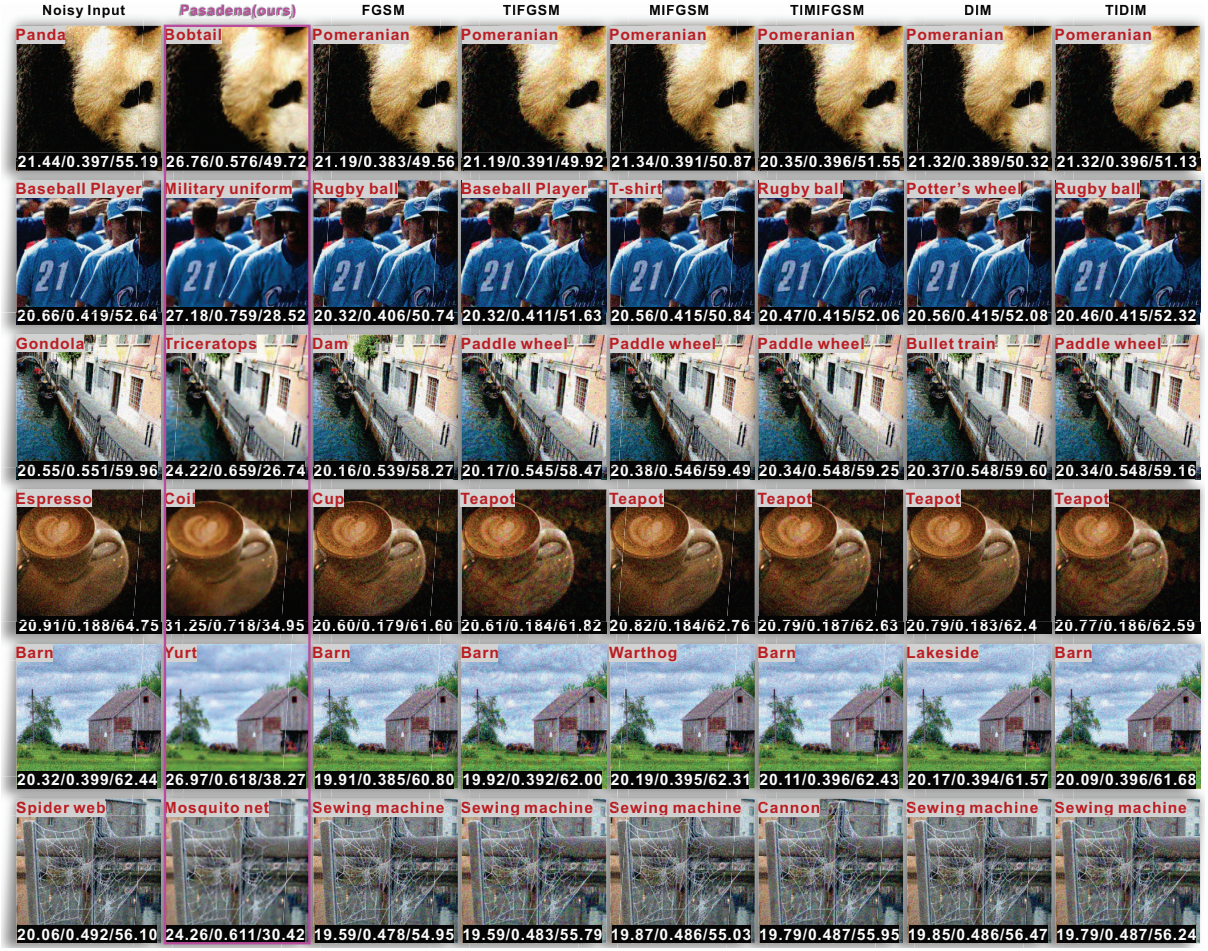


Figure 3: Visualization results of adversarial examples crafted for Inception-v4, using our method Pasadena and six baseline attacks. For each image, its prediction of Inception-v4 is displayed on top-left. Three numbers at the bottom refer to PSNR_L, SSIM and BRISQUE values. All noisy inputs are correctly classified to their ground truth label.

Table 1: Adversarial comparison results on NeurIPS'17 adversarial competition dataset with Additive Gaussian Noise ($\sigma=0.1$). It contains the success rates(%) of black&whitebox adversarial attacks among three normally trained models-Inc-v3, Inc-v4, IncRes-v2, using six baseline methods with $\epsilon = 8$ and our Pasadena. For each three columns, whitebox attack results are shown in the last one. The rest two columns display the blackbox attack results. We highlight the top three results with red, yellow and green, respectively.

Crafted from	Inc-v3			Inc-v4			IncRes-v2		
	Inc-v4	IncRes-v2	Inc-v3	Inc-v3	IncRes-v2	Inc-v4	Inc-v3	Inc-v4	IncRes-v2
FGSM	33.0	34.2	89.5	38.0	40.2	85.2	39.8	37.9	81.2
TIFGSM	26.6	22.4	83.1	23.7	25.8	77.7	25.9	28.5	73.4
MIFGSM	18.2	19.8	93.2	32.4	32.1	94.0	41.7	36.7	96.8
TIMIFGSM	23.0	20.3	92.9	24.7	27.0	92.8	30.6	35.3	93.8
DIM	48.3	49.2	94.3	56.6	57.7	94.1	63.1	60.4	95.1
TIDIM	39.8	35.0	91.7	35.4	40.2	90.8	40.6	47.1	89.6
Pasadena (ours)	64.0	62.8	88.2	66.6	66.9	93.9	69.8	73.4	92.1

Noted that some of TI attacking outputs have better BRISQUE values than noise inputs. The reason is that BRISQUE evaluates image according to its possible losses of “naturalness” by generalized Gaussian distribution. Other type of distortions would counteract “noise”. TI attacking method smooths the basic adversarial noise to

enhance its transferability. This operation yields a better BRISQUE score for the noise input.

4.2.2 *Qualitative Analysis.* Fig. 3 illustrates some adversarial examples of baselines and our framework. Our approach focuses on

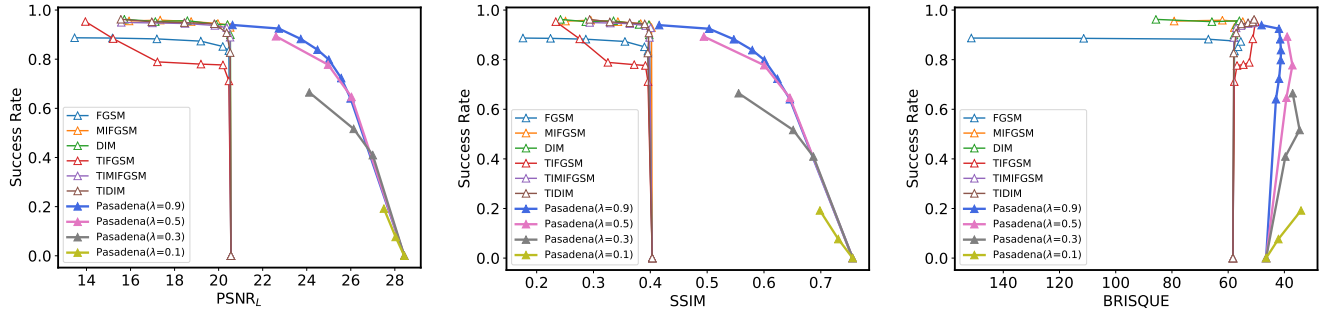


Figure 4: Whitebox attack success rate along with PSNR_L, SSIM and BRISQUE for six baseline methods with noise inputs and our four results (Pasadena) with different adversarial loss weights λ . Our curves are generated with threshold θ ranging from 0.05 to 0.65. From right to left, the points on baseline are corresponding to $\epsilon = 0, 4, 8, 16, 28, 42, 55$.

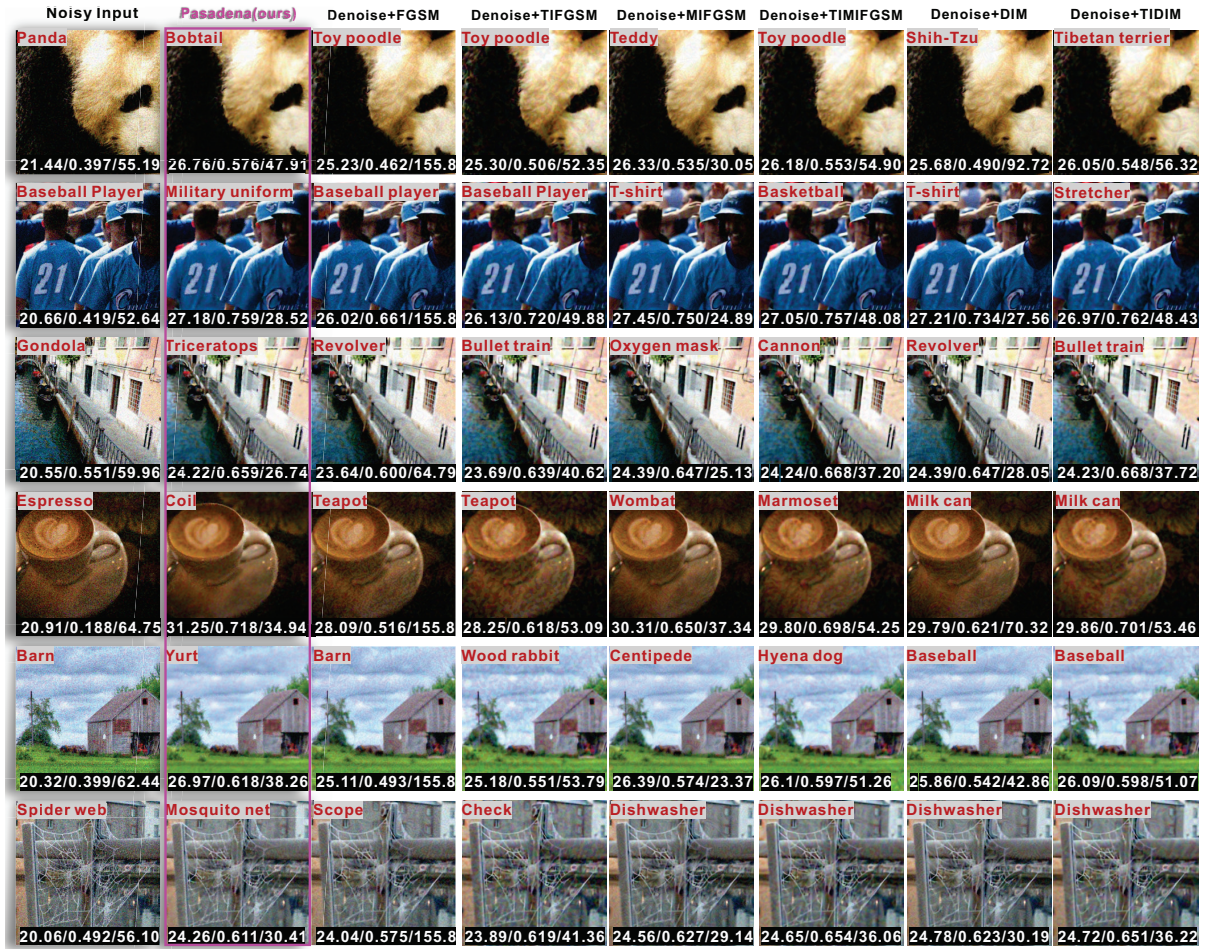


Figure 5: Visualization results of adversarial examples crafted for Inception-v4, using our method Pasadena and six baseline attacks. Different with Fig. 3, there is a denoising procedure (KPN) before baseline attacks. For each image, its prediction of Inception-v4 is displayed on top-left. Three numbers at the bottom refer to PSNR_L, SSIM and BRISQUE values. All noisy inputs are correctly classified to their ground truth label.

conducting the attack against to the edge area, which is more vulnerable than other part. This operation makes our method achieve the maximum attack with minimum perturbation. For example, the

TIMIFGSM attacks the first image of panda by perturbing every part and successfully misleads the prediction result as Pomeranian but poses a terrible image quality. However, during our attack changes

Table 2: Adversarial comparison results on NeurIPS’17 adversarial competition dataset with Additive Gaussian Noise ($\sigma=0.1$). It contains the success rates(%) of black&whitebox adversarial attacks among three normally trained models-Inc-v3, Inc-v4, IncRes-v2, using six baseline methods with $\epsilon = 8$ (denoised before attacked) and our Pasadena. For each three columns, whitebox attack results are shown in the last one. The rest two columns display the blackbox attack results. We highlight the top three results with red, yellow and green, respectively.

Crafted from	Inc-v3			Inc-v4			IncRes-v2		
Attacked model	Inc-v4	IncRes-v2	Inc-v3	Inc-v3	IncRes-v2	Inc-v4	Inc-v3	Inc-v4	IncRes-v2
Denoise+FGSM	9.1	12.1	77.6	10.9	14.2	67.2	11.9	11.2	62.2
Denoise+TIFGSM	4.4	4.0	60.2	0	4.7	45.1	0.2	8.9	46.1
Denoise+MIFGSM	12.3	14.1	97.3	19.0	21.8	98.3	29.9	25.5	100.0
Denoise+TIMIFGSM	8.9	6.1	96.6	6.3	11.0	97.4	13.3	23.6	96.4
Denoise+DIM	36.2	36.7	97.3	43.0	42.1	97.9	51.4	48.4	98.0
Denoise+TIDIM	24.4	16.4	93.4	16.6	21.2	94.2	21.6	34.5	91.1
Pasadena (ours)	64.0	62.8	88.2	66.6	66.9	93.9	69.8	73.4	92.1

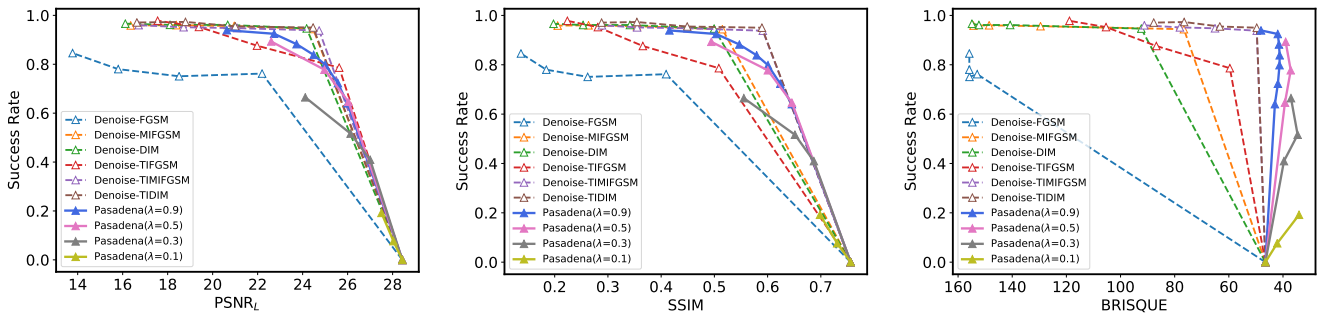


Figure 6: Whitebox attack success rate along with $PSNR_L$, SSIM and BRISQUE for six baseline methods with DENOISED inputs and our four results (Pasadena) with different adversarial loss weights λ . Our curves are generated with threshold θ ranging from 0.05 to 0.65. From right to left, the points on baseline are corresponding to $\epsilon = 0, 16, 28, 42, 55$.

prediction result to bobtail, it carries out another strategy which modifies the junction of its face and body in image. Moreover, it even depresses, rather than adds, noise on the non-edge part, and thereby resulting in a good image quality. Similar operation is also shown on the second image. Our method attacks only the edge of clothes and faces while baseline methods pollute all of the image and make the noise image noisier. For the image with obvious foreground object and contains rare edge, such as the fourth noisy input, our method produces excellent denoising result ($PSNR_L = 31.25$, $SSIM = 0.718$) with a success attack. However, the input with many edges or high frequency information may heavily depresses the performance of our edge detection method (See images in the third, fifth and last row). Our method thereby generates an indiscriminately attack for the entire image and results in low $PSNR_L$ and SSIM values. But we still achieve an improvement in image quality comparing with other attack methods.

4.2.3 Comparison on Transferability. To verify the transferability of our method, we conduct black-box attack experiment under the same image quality. For a fair comparison, we pick $\epsilon = 8$ for all baseline methods for their similar image quality.

Table 1 shows the blackbox and whitebox attacks results between three normally trained models. The first row shows the model from which we conduct the whitebox attack. Then we apply the whitebox attack results to other two blackbox models. The results show that our method achieves the highest transferability because

our method conducts the attack on the vulnerable part in image, i.e., the edge that is the common vulnerable area for most models. Nevertheless, adversarial noise on non-edge area may fail when it comes to different models.

4.3 Comparison with Denoise & Attack Baselines

4.3.1 Quantitative Analysis. We compare our method with denoise & attack baselines and show the results in Fig. 6. In terms of $PSNR_L$ and SSIM, our Pasadena with $\lambda = 0.9$ has higher $PSNR_L$ and SSIM than Denoise+FGSM and Denoise+TIFGSM under the similar success rates, but has slightly lower quality scores than other four baseline methods. However, when considering the BRISQUE measuring the naturalness of images, our method beats all six denoise & attack methods, which demonstrates the our method can generate more natural adversarial images.

4.3.2 Qualitative Analysis. We show six adversarial attack images in Fig. 5 with our Pasadena and six denoise & attack methods. Comparing with six baselines, our method can generate much better visualization results. For example, the ‘Panda’ case in the first row shows that our method maintains the denoising effect for non-edge regions (e.g., the face and body of panda), and only implements attack on the edge regions (e.g., the boundary across the black and white regions), leading to successful attack (e.g., classification result

Table 3: Varying denoising method and edge detector in our framework to conduct attacks among three normally trained models-Inc-v3, Inc-v4, IncRes-v2. For each three columns, whitebox attack results are shown in the last one. The rest two columns display the blackbox attack results. We highlight the results with different red intensities according to their success rates.

Crafted from	Inc-v3			Inc-v4			IncRes-v2		
Attacked model	Inc-v4	IncRes-v2	Inc-v3	Inc-v3	IncRes-v2	Inc-v4	Inc-v3	Inc-v4	IncRes-v2
Pasadena(Gau,Canny)	45.6	40.0	79.0	52.5	48.0	82.7	56.9	54.9	83.9
Pasadena(KPN,Canny)	55.9	53.9	82.9	62.5	60.6	90.4	64.1	62.6	88.4
Pasadena(Gau,BDCN)	57.3	54.6	85.1	62.9	61.0	92.2	66.4	67.4	89.9
Pasadena(KPN,BDCN)	64.0	62.8	88.2	66.6	66.9	93.9	69.8	73.4	92.1

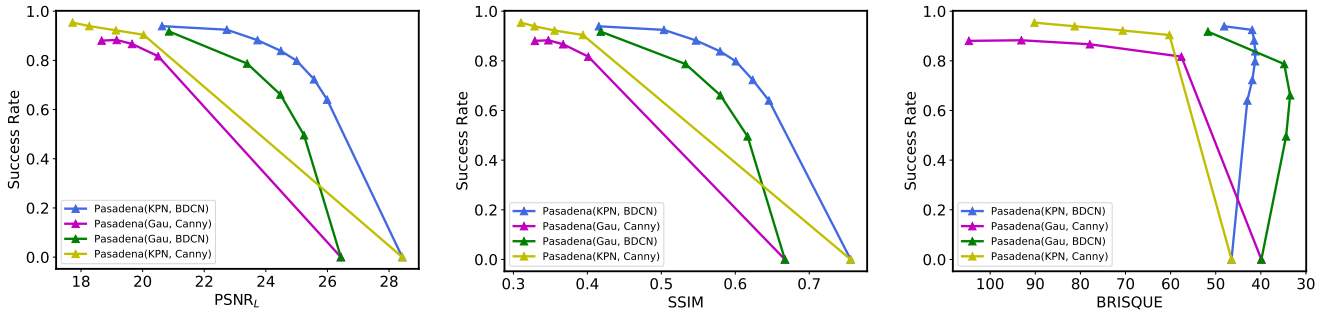


Figure 7: Whitebox attack success rate along with $PSNR_L$, SSIM and BRISQUE for our framework with different choice of denoising and edge detector methods. KPN refers to the denoising method proposed in [25]. Gau means Gaussian kernel is selected in our denoising part. Canny and BDCN are edge detecting methods of [3] and [13], respectively. The dots with zero success rate represent the performance of denoising results using KPN (blue and yellow) and Gaussian kernel (green and purple).

from ‘Panda’ to ‘Bobtail’) while better visualization (*i.e.*, higher $PSNR_L$, SSIM, and lower BRISQUE).

In contrast, the denoise & attack methods perturb the entire denoised image and result in re-corrupted images with obvious noise textures, although they might achieve higher $PSNR_L$ and SSIM than our method. Specifically, the Denoise+TIFGSM/TIMIFGSM/TIDIM methods produce salient noise texture on all images, although they have similar $PSNR_L$ and SSIM with our method. Moreover, some of the baselines fail to mislead the input images. For example, Denoise+FGSM/TIFGSM do not change the predicted category of the input ‘basketball player’ image.

4.3.3 Comparison on Transferability. To further verify the transferability of our methods, we conduct a transferability experiment with the same setting of Sec. 4.2.3 and show the whitebox attacking results as well as their corresponding transferability across three normally trained models in Table 2. It is easy to see that our method achieves the highest transferability for all subject models, *i.e.*, Inc-v3, Inc-v4, and IncRes-v2. Specifically, in terms of the subject model Inc-v3, *i.e.*, adversarial attacking results crafted from Inception-v3, TIMIFGSM has the highest whitebox attacking success rate of 94.3%, while our method has slightly worse result with 88.2%. However, when considering the transferability of Denoise+TIMIFGSM, *i.e.*, the success rate of using adversarial examples to attack Inc-v4 and IncRes-v2, its success rates *i.e.*, 48.3% and 49.2%, are much lower than that of our method, *i.e.*, 66.6% and 66.9%. We find similar adversarial results crafted for other two models, which draws the the same conclusion with Sec. 4.2.3, *i.e.*, our adversarial attacking results have the highest transferability over all baselines.

4.4 Ablation Study

In this section, we exhibit the results of our framework with different choice of denoising and edge detector methods. To be specific, we choose two methods for each part in our framework, *i.e.*, KPN [25] and Gaussian kernel for denoising part, Canny operator [3] and BDCN [13] for edge detecting part. As Canny operator generates edge map with 1-pixel width, we apply a dilation operation before feeding it into our framework. During the implementation, we choose four dilation sizes, denoted as canny width $CannyW$, uniformly ranging from 3 to 9. We also choose four thresholds θ for BDCN methods, *i.e.*, 0.05, 0.25, 0.45, 0.65.

4.4.1 Quantitative Analysis. Fig. 7 illustrates the performance of our framework with different denoising methods and edge detectors. KPN (blue and yellow curves) exhibits a better ability in keeping image quality than Gaussian kernel (green and purple curves). Blue-green lines pair and yellow-purple lines pair both illustrate that higher image quality is inherited from better denoising results. Note that there are three points of purple, green and blue which have a similar attack success rate of 0.8 with giant difference in terms of image quality. Among these points, purple group (Gaussian and Canny) holds the worst SSIM and $PSNR_L$ values around 0.4 and 20. Comparing with Gaussian and BDCN group (green), BDCN outperforms Canny to a great extend. The blue point of group KPN and BDCN is the best in image quality, which further confirms the positive effect of KPN.

4.4.2 Qualitative Analysis. Fig. 8 lists three groups of adversarial examples using different combination of denoising methods and



Figure 8: Visualization results of adversarial examples crafted for Inception-v4, using our method Pasadena with different denoising methods and edge detectors. The denoising methods are KPN [25] and Gaussian kernel (kernel size=5, $\sigma = 1$), while edge detectors are BDCN and Canny. Combining form is list at top of each group. For each image, its prediction of Inception-v4 is displayed on top-left. Three numbers at the bottom refer to PSNR_L, SSIM and BRISQUE values.

edge detectors. The combination of KPN and BDCN successfully attack the inputs as well as keeping the best image quality. The leaf and desk are more clear in two KPN groups. Same situation also occurs in the wall of the second case, and the cloth of the third case. In addition, comparing the attack area of the third input, (Gau, Canny) pollutes the face of rightmost person. But (Gau, BDCN) denoises most area of face and only perturbs the edge. That means BDCN can precisely locate vulnerable area while keeping the denoising effect for the no-edge part.

4.4.3 Comparison on transferability. To further study the influence of each part to the transferability, we use a similar hyperparameters selection strategy as the former experiment in Sec 4.2.3. $CannyW = 3$ and $\theta = 0.05$ are thereby picked for they share the similar SSIM values near 0.4 in Fig 7. Table 3 shows the results which draw the same conclusion with Sec. 4.4. Combination of KPN and BDCN outperforms other groups in both whitebox attacks and blackbox attacks, which further proves that better denoising and edge detecting results enhance our final performance. Specifically, our framework benefits from excellent denoising ability of KPN and generate more powerful adversarial examples in high image qualities. However, Gaussian kernel losing its denoising ability too early before our framework reaches higher attack success rate. In addition, BDCN helps our framework focus its attack on vulnerable area by its precise edge locating ability. While Canny edge generates too much non-effective attacking area which sacrifices image quality without any increase on attack success rate.

5 CONCLUSIONS

In this work, we have investigated a new task named as *adversarial denoise attack* that stealthily embeds the attacks inside the image denoising module. Thus it can simultaneously denoise input images

while fooling the state-of-the-art deep models. We have formulated this new task as a kernel prediction problem and proposed the *adversarial-denoising kernel prediction* that can produce adversarial-noiseless kernels for effective denoising and adversarial attacking simultaneously. Furthermore, we have implemented an adaptive *perceptual region localization* to identify the semantic-related vulnerability regions with which the attack can be more effective while not doing too much harm to the denoising. Thus, our proposed method is termed as *Pasadena* (Perceptually Aware and Stealthy Adversarial DENoise Attack). We have validated our method on the NeurIPS'17 adversarial competition dataset and demonstrated that our method not only realizes denoising but has advantages of high success rate and transferability over the state-of-the-art attacks. In future, it is interested to explore the interplay between Pasadena and other novel additive and non-additive adversarial attack modes [10, 11, 42] as well as in tandem with the potential improvement on the attack and defense mechanisms [19, 20, 32, 43, 44] surrounding the imminent DeepFake problems.

REFERENCES

- [1] Evan Ackerman. 2017. How drive. ai is mastering autonomous driving with deep learning. *IEEE Spectrum Magazine* 1 (2017).
- [2] Steve Bako, Thijs Vogels, Brian McWilliams, Mark Meyer, Jan Novák, Alex Harvill, Pradeep Sen, Tony Deroose, and Fabrice Rousselle. 2017. Kernel-Predicting Convolutional Networks for Denoising Monte Carlo Renderings. *ACM Trans. Graph.* 36, 4, Article 97 (July 2017), 14 pages. <https://doi.org/10.1145/3072959.3073708>
- [3] John Canny. 1986. A computational approach to edge detection. *IEEE Transactions on pattern analysis and machine intelligence* 6 (1986), 679–698.
- [4] Xinyuan Chen, Li Song, and Xiaokang Yang. 2016. Deep rnns for video denoising. In *Applications of Digital Image Processing XXXIX*, Vol. 9971. International Society for Optics and Photonics, 99711T.
- [5] Kostadin Dabov, Alessandro Foi, Vladimir Katkovnik, and Karen Egiazarian. 2007. Image denoising by sparse 3-D transform-domain collaborative filtering. *IEEE Transactions on image processing* 16, 8 (2007), 2080–2095.
- [6] Yinpeng Dong, Fangzhou Liao, Tianyu Pang, Hang Su, Jun Zhu, Xiaolin Hu, and Jianguo Li. 2018. Boosting adversarial attacks with momentum. In *Proceedings of the IEEE conference on computer vision and pattern recognition*. 9185–9193.
- [7] Yinpeng Dong, Tianyu Pang, Hang Su, and Jun Zhu. 2019. Evading defenses to transferable adversarial examples by translation-invariant attacks. In *Proceedings of the IEEE Conference on Computer Vision and Pattern Recognition*. 4312–4321.
- [8] Michaël Gharbi, Gaurav Chaurasia, Sylvain Paris, and Frédo Durand. 2016. Deep joint demosaicking and denoising. *ACM Transactions on Graphics (TOG)* 35, 6 (2016), 1–12.
- [9] Ian J Goodfellow, Jonathon Shlens, and Christian Szegedy. 2014. Explaining and harnessing adversarial examples. *arXiv preprint arXiv:1412.6572* (2014).
- [10] Qing Guo, Felix Juefei-Xu, Xiaofei Xie, Lei Ma, Jian Wang, Bing Yu, Wei Feng, and Yang Liu. 2020. ABBA: Saliency-Regularized Motion-Based Adversarial Blur Attack. *arXiv preprint arXiv:2002.03500* (2020).
- [11] Qing Guo, Xiaofei Xie, Felix Juefei-Xu, Lei Ma, Zhongguo Li, Wanli Xue, Wei Feng, and Yang Liu. 2020. SPARK: Spatial-aware Online Incremental Attack Against Visual Tracking. In *Proceedings of the European Conference on Computer Vision (ECCV)*.
- [12] Qiang Guo, Caiming Zhang, Yunfeng Zhang, and Hui Liu. 2015. An efficient SVD-based method for image denoising. *IEEE transactions on Circuits and Systems for Video Technology* 26, 5 (2015), 868–880.
- [13] J. He, S. Zhang, M. Yang, Y. Shan, and T. Huang. 2019. Bi-Directional Cascade Network for Perceptual Edge Detection. In *2019 IEEE/CVF Conference on Computer Vision and Pattern Recognition (CVPR)*. 3823–3832.
- [14] Kaiming He, Xiangyu Zhang, Shaoqing Ren, and Jian Sun. 2016. Deep residual learning for image recognition. In *Proceedings of the IEEE conference on computer vision and pattern recognition*. 770–778.
- [15] Felix Heide, Steven Diamond, Matthias Nießner, Jonathan Ragan-Kelley, Wolfgang Heidrich, and Gordon Wetzstein. 2016. Proximal: Efficient image optimization using proximal algorithms. *ACM Transactions on Graphics (TOG)* 35, 4 (2016), 1–15.
- [16] Felix Heide, Markus Steinberger, Yun-Ta Tsai, Mushfiqur Rouf, Dawid Pająk, Dikpal Reddy, Orazio Gallo, Jing Liu, Wolfgang Heidrich, Karen Egiazarian, et al. 2014. Flexisp: A flexible camera image processing framework. *ACM Transactions on Graphics (TOG)* 33, 6 (2014), 1–13.

- [17] Geoffrey Hinton, Li Deng, Dong Yu, George E Dahl, Abdel-rahman Mohamed, Navdeep Jaitly, Andrew Senior, Vincent Vanhoucke, Patrick Nguyen, Tara N Sainath, et al. 2012. Deep neural networks for acoustic modeling in speech recognition: The shared views of four research groups. *IEEE Signal processing magazine* 29, 6 (2012), 82–97.
- [18] Gao Huang, Zhuang Liu, Laurens Van Der Maaten, and Kilian Q Weinberger. 2017. Densely connected convolutional networks. In *Proceedings of the IEEE conference on computer vision and pattern recognition*. 4700–4708.
- [19] Yihao Huang, Felix Juefei-Xu, Run Wang, Qing Guo, Lei Ma, Xiaofei Xie, Jianwen Li, Weikai Miao, Yang Liu, and Geguang Pu. 2020. FakePolisher: Making DeepFakes More Detection-Evasive by Shallow Reconstruction. *arXiv preprint arXiv:2006.07533* (2020).
- [20] Yihao Huang, Felix Juefei-Xu, Run Wang, Qing Guo, Xiaofei Xie, Lei Ma, Jianwen Li, Weikai Miao, Yang Liu, and Geguang Pu. 2020. FakeLocator: Robust Localization of GAN-Based Face Manipulations. *arXiv preprint arXiv:2001.09598* (2020).
- [21] Alexey Kurakin, Ian Goodfellow, Samy Bengio, Yinpeng Dong, Fangzhou Liao, Ming Liang, Tianyu Pang, Jun Zhu, Xiaolin Hu, Cihang Xie, et al. 2018. Adversarial attacks and defences competition. In *The NIPS'17 Competition: Building Intelligent Systems*. Springer, 195–231.
- [22] Ding Liu, Bihan Wen, Xianming Liu, Zhangyang Wang, and Thomas S. Huang. [n.d.]. When image denoising meets high-level vision tasks: A deep learning approach. In *Proceedings of the 27th International Joint Conference on Artificial Intelligence, IJCAI 2018*. 842–848.
- [23] Florian Luisier, Thierry Blu, and Michael Unser. 2010. SURE-LET for orthonormal wavelet-domain video denoising. *IEEE Transactions on Circuits and Systems for Video Technology* 20, 6 (2010), 913–919.
- [24] Matteo Maggioni, Giacomo Boracchi, Alessandro Foi, and Karen Egiazarian. 2011. Video denoising using separable 4D nonlocal spatiotemporal transforms. In *Image Processing: Algorithms and Systems IX*, Vol. 7870. International Society for Optics and Photonics, 787003.
- [25] B. Mildenhall, J. T. Barron, J. Chen, D. Sharlet, R. Ng, and R. Carroll. 2018. Burst Denoising with Kernel Prediction Networks. In *2018 IEEE/CVF Conference on Computer Vision and Pattern Recognition*. 2502–2510.
- [26] Anish Mittal, Anush Krishna Moorthy, and Alan Conrad Bovik. 2012. No-reference image quality assessment in the spatial domain. *IEEE Transactions on image processing* 21, 12 (2012), 4695–4708.
- [27] Seyed-Mohsen Moosavi-Dezfooli, Alhussein Fawzi, and Pascal Frossard. 2016. Deepfool: a simple and accurate method to fool deep neural networks. In *CVPR*. 2574–2582.
- [28] Seyed-Mohsen Moosavi-Dezfooli, Ashish Shrivastava, and Oncel Tuzel. 2018. Divide, denoise, and defend against adversarial attacks. *arXiv preprint arXiv:1802.06806* (2018).
- [29] Maryam M Najafabadi, Flavio Villanustre, Taghi M Khoshgoftaar, Naeem Seliya, Randall Wald, and Edin Muharemagic. 2015. Deep learning applications and challenges in big data analytics. *Journal of Big Data* 2, 1 (2015), 1.
- [30] Nicolas Papernot, Patrick McDaniel, Arunesh Sinha, and Michael Wellman. 2016. Towards the science of security and privacy in machine learning. *arXiv preprint arXiv:1611.03814* (2016).
- [31] Pietro Perona and Jitendra Malik. 1990. Scale-space and edge detection using anisotropic diffusion. *IEEE Transactions on pattern analysis and machine intelligence* 12, 7 (1990), 629–639.
- [32] Hua Qi, Qing Guo, Felix Juefei-Xu, Xiaofei Xie, Lei Ma, Wei Feng, Yang Liu, and Jianjun Zhao. 2020. DeepRhythm: Exposing DeepFakes with Attentional Visual Heartbeat Rhythms. *arXiv preprint arXiv:2006.07634* (2020).
- [33] SM Mahbubur Rahman, M Omair Ahmad, and MNS Swamy. 2007. Video denoising based on inter-frame statistical modeling of wavelet coefficients. *IEEE Transactions on Circuits and Systems for Video Technology* 17, 2 (2007), 187–198.
- [34] Qing Rao and Jelena Frtunikj. 2018. Deep learning for self-driving cars: chances and challenges. In *Proceedings of the 1st International Workshop on Software Engineering for AI in Autonomous Systems*. 35–38.
- [35] Leonid I Rudin, Stanley Osher, and Emad Fatemi. 1992. Nonlinear total variation based noise removal algorithms. *Physica D: nonlinear phenomena* 60, 1-4 (1992), 259–268.
- [36] Jiawei Su, Danilo Vasconcellos Vargas, and Kouichi Sakurai. 2019. One pixel attack for fooling deep neural networks. *IEEE Transactions on Evolutionary Computation* (2019).
- [37] Shuochen Su, Mauricio Delbracio, Jue Wang, Guillermo Sapiro, Wolfgang Heidrich, and Oliver Wang. 2017. Deep video deblurring for hand-held cameras. In *Proceedings of the IEEE Conference on Computer Vision and Pattern Recognition*. 1279–1288.
- [38] Christian Szegedy, Sergey Ioffe, Vincent Vanhoucke, and Alexander A Alemi. 2017. Inception-v4, inception-resnet and the impact of residual connections on learning. In *Thirty-first AAAI conference on artificial intelligence*.
- [39] Christian Szegedy, Vincent Vanhoucke, Sergey Ioffe, Jon Shlens, and Zbigniew Wojna. 2016. Rethinking the inception architecture for computer vision. In *Proceedings of the IEEE conference on computer vision and pattern recognition*. 2818–2826.
- [40] Christian Szegedy, Wojciech Zaremba, Ilya Sutskever, Joan Bruna, Dumitru Erhan, Ian Goodfellow, and Rob Fergus. 2013. Intriguing properties of neural networks. *arXiv preprint arXiv:1312.6199* (2013).
- [41] Xin Tao, Hongyun Gao, Renjie Liao, Jue Wang, and Jiaya Jia. 2017. Detail-revealing deep video super-resolution. In *Proceedings of the IEEE International Conference on Computer Vision*. 4472–4480.
- [42] Run Wang, Felix Juefei-Xu, Qing Guo, Yihao Huang, Xiaofei Xie, Lei Ma, and Yang Liu. 2019. Amora: Black-box Adversarial Morphing Attack. *arXiv preprint arXiv:1912.03829* (2019).
- [43] Run Wang, Felix Juefei-Xu, Yihao Huang, Qing Guo, Xiaofei Xie, Lei Ma, and Yang Liu. 2020. DeepSonar: Towards Effective and Robust Detection of AI-Synthesized Fake Voices. *arXiv preprint arXiv:2005.13770* (2020).
- [44] Run Wang, Felix Juefei-Xu, Lei Ma, Xiaofei Xie, Yihao Huang, Jian Wang, and Yang Liu. 2020. FakeSpotter: A Simple yet Robust Baseline for Spotting AI-Synthesized Fake Faces. *International Joint Conference on Artificial Intelligence (IJCAI)* (2020).
- [45] Zhou Wang, Alan C Bovik, Hamid R Sheikh, and Eero P Simoncelli. 2004. Image quality assessment: from error visibility to structural similarity. *IEEE transactions on image processing* 13, 4 (2004), 600–612.
- [46] Cihang Xie, Zhishuai Zhang, Yuyin Zhou, Song Bai, Jianyu Wang, Zhou Ren, and Alan L Yuille. 2019. Improving transferability of adversarial examples with input diversity. In *Proceedings of the IEEE Conference on Computer Vision and Pattern Recognition*. 2730–2739.
- [47] Kai Zhang, Wangmeng Zuo, Yunjin Chen, Deyu Meng, and Lei Zhang. 2017. Beyond a gaussian denoiser: Residual learning of deep cnn for image denoising. *IEEE Transactions on Image Processing* 26, 7 (2017), 3142–3155.